Long-term carbon transport and fuel retention in gaps of the main toroidal limiter in TEXTOR

A. Kreter[a*], P. Wienhold[a], H.G. Esser[a], A. Litnovsky[a],

V. Philipps[a], K. Sugiyama[b] and TEXTOR team

[a]*Institute for Energy and Climate Research - Plasma Physics, Forschungszentrum Jülich, Association EURATOM-FZJ, Trilateral Euregio Cluster, Germany*

[b]*Max-Planck-Institut für Plasmaphysik, EURATOM Association, 85748 Garching, Germany*

Abstract

The 1.1-1.5 mm wide gaps between tiles of the main toroidal belt limiter in TEXTOR were utilized to study the long-term impurity deposition and fuel retention in gaps. The tiles were exposed during a full tokamak campaign of 9365 s of plasma to various discharge conditions and wall conditioning, accumulating of up to 30 μm thick layers at the gap entrance. It was found that (i) gaps trap impurities twice as efficient as the top surface, (ii) the deposition in the toroidal gaps is twice as high as in the poloidal, (iii) carbon deposition decays with a fall-off length of about 0.7 mm towards the gap bottom, (iv) deposition on the bottom is significantly higher than on the adjacent side walls of gaps, (v) the amount of deuterium scales with the amount of carbon with D/C varying from 3% to 30% depending on the surface temperature.

PACS: 28.52.Fa, 52.40.Hf, 52.55.Fa

PSI-20 keywords: Carbon impurities, Erosion & Deposition, Retention, Surface analysis, TEXTOR

* *Corresponding author address:* Forschungszentrum Jülich, IEK-4, 52425 Jülich, Germany

* *Corresponding author E-mail:* A.Kreter@fz-juelich.de

Presenting author: Arkadi Kreter

Presenting author E-mail: A.Kreter@fz-juelich.de

1. Introduction

In ITER all plasma-facing components will be castellated in order to reduce eddy currents and thermo-mechanical stresses on the wall materials. Gaps between castellation cells serve, however, as traps for the migrating impurities and co-deposited fuel, contributing to the safety problem of the tritium retention [1]. The efficiency of the fuel removal methods is restricted in gaps due to their geometry [2-4]. A dedicated campaign to study the mechanisms of fuel retention was performed in the Tore Supra tokamak, revealing the details of the asymmetry of the deposition in toroidal and poloidal gaps [5] and peculiarities of the co-deposition in gaps [6]. Several dedicated short-term experiments were performed on the TEXTOR tokamak [7-9] investigating the contribution of the co-deposition in gaps to the overall fuel retention. In these experiments, carbon was deposited in gaps regardless whether the top surface was erosion or deposition dominated. The deposition was higher at the gap entrance, decaying towards the gap bottom with an e-folding length of 1.0-1.8 mm. On the gap bottom, the deposition was significantly higher than on the adjacent side walls of the gap. The modelling with the Monte-Carlo impurity tracing code 3D-GAPS reasonably reproduced the experimental results [10].

The dedicated studies are typically performed in the frame of a single experiment. Therefore, the results are only representative for the particular experimental conditions, e.g. the plasma density and temperature, the magnetic field configuration, the confinement regime and the sample surface temperature.

The aim of the present study was to investigate the long-term carbon transport and fuel retention in gaps over a variety of discharge conditions and wall conditioning procedures representative for an entire TEXTOR operation campaign. The gaps between specially prepared graphite tiles of the main toroidal belt limiter in TEXTOR were utilized for the study.

2. Experimental

TEXTOR is a medium size tokamak (major radius 1.75 m, minor radius 0.46 cm) with a circular poloidal plasma cross-section [11]. The position of the last closed flux surface (LCFS) is defined by the toroidal belt limiter ALT-II (Advanced Limiter Test II) [12]. ALT-II consists of 8 blades, each carrying 28 tiles ordered in two poloidal rows, with a total surface area of 3.4 m^2 (Fig. 1 (a)). The tiles are made of the fine-grain isotropic graphite. They have a refined poloidal shape of a double-roof-like geometry with a roof inclination, or an angle of incidence of the magnetic field lines, continuously increasing from <0.1° in the center to 2.5° at the edge. This geometry extends the region with an angle of incidence of the magnetic field of less than 1° to 10 mm in the scrape-off layer, resulting in a spread of the heat flux to a larger effective area [13]. Toroidally the tiles are shaped according to the toroidal curvature of the LCFS. The tile shaping leads to the net-deposition of carbon in the central poloidal part of the limiter (about one third of the limiter area), where the angle of incidence of the magnetic field is shallower [14-16]. To the edges, the limiter surface is typically erosion dominated. The erosion-deposition pattern is also subjected to the magnetic field ripple [13], causing inhomogeneities in the erosion-deposition pattern from tile to tile.

Tiles 20 and 21 of blade 5 were specially prepared to investigate the deposition in gaps formed with adjacent tiles (Fig. 1 (a,b)). They were hand-polished to an average roughness of 0.1 μm and coated with a 300 nm Si layer, causing coloured interference fringes on the tiles in day light illumination. Silicon acted as a marker to discriminate deposits from the bulk material. The tiles had a size of 100×155 mm^2 in the toroidal and poloidal directions, respectively. The toroidal and poloidal gap widths were 1.5 and 1.1 mm, respectively. The gap depth corresponded to the tile height, which was 10 mm in the center and decreased to zero at the edge. A stainless steel foil was placed under tiles 20 and 21 covering the bottom of the poloidal gap between the tiles, schematically shown in Fig. 1 (b). The experimental campaign of TEXTOR included 9365 s of plasma and 7 boronizations. The boronizations

were performed by the glow discharge in diborane B_2H_6. The area-averaged hydrogen fluence to the limiter during tokamak discharges was 3×10^{25} m^{-2}. The ALT-II limiter temperature between pulses corresponds to the liner temperature of 150°C. During the tokamak operation, there are excursions of the surface temperature of the tiles up to 400°C [17], while the temperature of the limiter support structure does not exceed 200°C.

After the campaign, the tiles were dismounted (Fig. 1 (c,d)) and analysed by various post-mortem techniques. Scanning Electron Microscopy (SEM) and optical microscopy were used to determine the layer thickness of >~1 μm. To determine the thickness, the segments along the tile gaps were separated from the central part of the tile, then cut and polished across the gap surface. Depth profiles of elements in the films were measured by Secondary Ion Mass Spectrometry (SIMS). Rutherford Backscattering Spectrometry (RBS) and Electron Probe Microanalysis (EPMA) were applied for the absolute amounts of elements constituting the deposits, with the exception of deuterium, which was measured by Nuclear Reaction Analysis (NRA). Thickness determination by the interference fringe analysis in the transparent regions completed the investigations. The analyses were done at several positions for both poloidal and the toroidal gaps, as well as for the foil at the bottom between tiles 20 and 21.

3. Results

The visual appearance of the tiles after the exposure in TEXTOR (Fig. 1 (c,d)) exhibits the typical erosion-deposition pattern for the top surface of ALT-II, with the net-deposition for the central ≈1/3 of the area, above the bolt holes, and the net-erosion towards the poloidal edge. The deposition thickness on tile 20 was up to ~10 μm, while on tile 21 it was of maximum ~1 μm due to the field ripple. A visible deposition in the gaps was found at all toroidal and poloidal positions.

The deposits at the entrance to the gap were thick enough to be observed by optical

microscopy. Fig. 2(a) shows an example of the layer thickness in the toroidal gap decaying from 26 μm at the entrance to 12 μm at 0.4 mm into the gap. It is not visible at 4 mm. Note that the 0.3 μm thick Si marker layer is visible as a bright line from the top surface towards deep into the gap. The Si layer was not affected by the plasma operation, as the area shown here was in the net-deposition zone. Deposits in the poloidal gap are less thick, but behave similar (Fig. 2(b)).

The thickness profiles along the gaps for several positions are summarized in Fig. 3. Values obtained from the optical microscopy are well completed by SIMS (Fig. 3 (a)). The RBS values of areal atomic density of elements were for comparison converted to the thickness assuming a constant film density of 6.5×10^{22} at./cm^3 (Fig. 3 (b)). Taking into account that the RBS measurement spots are of 1×1 mm^2, comparable with the decay length of the layer thickness, the agreement of the thickness from RBS and other methods within a factor of 2 is reasonable. The results are confirmed by the thickness analysis of the colour fringes in the transparent parts of the deposit. A deposition thickness of up to 20-30 μm was measured at the entrance of the toroidal gaps for both tiles, despite a difference in deposition on the top surface of ~10 μm and ~1 μm for tiles 20 and 21, respectively. The amount of deposition in the toroidal gap is, depending on the position, at least by a factor 2 higher than in the poloidal gap. The thickness decays with an e-folding length between 0.5 and 0.9 mm with an average value of 0.7 mm, indicated in Fig. 3 (a). Fig. 3 also illustrates that the deposition on the opposite sides of the poloidal gap between tiles 20 and 21 is symmetric. No data is available on the deposition symmetry in the toroidal gap, as the tiles from the ALT-II upper row, complementing the toroidal gap, were not analysed. In the poloidal gap, the deposition continuously increases from the limiter edge towards the center. The RBS data show that, normalizing the sum of carbon, boron and oxygen atoms to 100%, carbon contributes with ≈90 at.% at the gap entrance, with its fraction decaying towards the gap

bottom. There is virtually no carbon on the side walls below 5 mm into the gap. Whereas the amount of carbon decreases exponentially, the boron fall-off is close to the linear dependence. Deep in the gap boron dominates the deposition. The ratio of oxygen (not shown in the figure) to boron is ≈1.5, indicating the formation of stable oxide B_2O_3 due to the gettering.

A visible stripe of 1.1 mm width was found on the foil exposed under tiles 20 and 21, corresponding to the deposition on the poloidal gap bottom (Fig. 4 (a)). The layer thickness of ≈1.1 μm, shown as a bar on Fig. 3 (a), is quite uniform. RBS and EPMA found the layer consisting of 60 at.% boron, 20 at.% carbon and 20 at.% oxygen (Fig. 3 (b)). The film delaminated from the foil (Fig. 4 (b)) exhibits a stratified structure, probably corresponding to 7 boronizations during the campaign. The SIMS depth profile of the deposit (Fig. 4 (c)) confirms the sequence of boron and carbon rich sub-layers, corresponding to the boronizations and the tokamak operation, respectively.

The amount of deuterium close to the gap entrance correlates to the amount of carbon with a D/C ratio of 3%-10%, similar to the ratio at the top surface. At the gap bottom a D/C ratio of 30% was found. This can be attributed to the lower temperature excursions during the tokamak pulses for the gap bottom in comparison with the top surface. A fraction of deuterium on the gap bottom can also be stored in boron, which is the dominating species there.

4. Summary and discussion

The carbon deposition rates at the gap entrance of up to 3 nm/s are similar to the maximum values found on the top surface of the ALT-II limiter [14-16]. However, the rates decay with a characteristic length of about 0.7 mm towards the bottom. This fall-off length is shorter than the lengths found in the dedicated short-term experiments in TEXTOR despite significantly larger gap widths for the ALT-II limiter, 1.5 mm toroidal and 1.1 mm poloidal, in comparison to the dedicated experiments of typically 0.5 mm [7-9]. About 4 mm deep in

the ALT-II gap essentially no carbon was detectible. The deposit there was dominated by boron stemming from boronizations by glow discharges in B_2H_6. Earlier studies [2] indicated that in glow discharges, in absence of the magnetic field, ions penetrate in the gap with a higher efficiency.

The amount of deposition in the toroidal gap is by a factor of ≈2 higher than in the poloidal. The higher trapping efficiency of the toroidal gaps is consistent with the observations in the short-term experiments [7-9]. The deeper penetration of the magnetic field lines in the toroidal than in poloidal gaps is probably the main reason for this effect. The roof-like geometry of the ALT-II limiter leads to the step-wise transport of carbon towards the limiter tip, the position of the toroidal gap [14-16]. This can intensify to the deposition in the toroidal gap.

In the short-term experiments [7], a larger amount of carbon was deposited in the gap when the top surface was in the erosion dominated than in the deposition dominated regime. This is in the apparent contradiction with the ALT-II limiter, where a higher deposition was found in the poloidal gaps close to the limiter center, being the net-deposition zone, than at positions towards the tile edge, where the erosion dominates the top surface. The erosion-deposition balance on the top surface is obviously not the defining mechanism for the amount of the deposition in the gap. It is rather the flux of carbon into the gap, which was higher in the erosion dominated region for the dedicated experiments and in the deposition zone for the ALT-II limiter.

On the gap bottom, only 20% of 1.1 μm total deposition was carbon. The main contributor was boron from the boronizations. Still, the amount of carbon deposited on the bottom was significantly higher than on the adjacent side walls of the gap. This special role of the gap bottom confirms the findings from the dedicated experiments [7-9]. The role of the gap bottom can be quantified by its contribution to the total deposition in the gap. For position

1 of the poloidal gap (Fig. 1 (d)) the value is 2% for carbon and 30% for boron. The value for boron underlines the high gap penetration efficiency of ions in the glow discharges. For carbon, the value is in a good agreement with the recent quartz microbalance studies in TEXTOR, whereas in the previous dedicated experiments it was significantly higher [10].

The carbon deposition rates were determined at different position in the poloidal and toroidal gaps of ALT-II. The integral carbon deposition rate in the gaps scaled-up for the entire ALT-II limiter is 8×10^{-5} g/s, which is 2.8% of the deposition rate on the limiter surface. The fraction of the gap entrance area to the total limiter area is 1.5%, meaning that, on average, gaps trap carbon almost twice as efficiently as the top surface. In ITER, the gap entrance area contributes with ≈10% to the total surface area. Assuming the same gap trapping efficiency similar to TEXTOR, about 20% of re-deposited impurities along with co-deposited tritium will be stored in gaps. Although this estimate is rather crude, it underlines the important role of gaps concerning the fuel retention and calls for the further efforts developing the techniques for the efficient fuel removal from gaps.

References

[1] K. Krieger, W. Jacob, D.L. Rudakov et al., J. Nucl. Mater. 363-365 (2007) 870.

[2] C. Schulz, A. Kreter, V. Philipps, A. Litnovsky and U. Samm, J. Nucl. Mater. 415 (2011) S781.

[3] T. Schwarz-Selinger, U. von Toussaint, C. Hopf and W. Jacob, Phys. Scr. T138 (2009) 014009.

[4] I. Tanarro, J.A. Ferreira, V.J. Herrero et al., J. Nucl. Mater. 390-391 (2009) 696.

[5] C. Martin, R. Ruffe, C. Pardanaud et al., J. Nucl. Mater. 415 (2011) S258.

[6] T. Dittmar, E. Tsitrone, B. Pégourié et al., J. Nucl. Mater. 415 (2011) S757.

[7] A. Litnovsky, P. Wienhold, V. Philipps et al., J. Nucl. Mater. 415 (2011) S289.

[8] A. Litnovsky, P. Wienhold, V. Philipps et al., J. Nucl. Mater. 390-391 (2009) 556.

[9] A. Litnovsky, V. Philipps, A. Kirschner et al., J. Nucl. Mater. 367-370 (2007) 1481.

[10] D. Matveev, these proceedings, P2-40.

[11] U. Samm, Fusion Sci. Technol. 47 (2005) 73.

[12] K. H. Finken, D. Reiter, T. Denner et al., Fusion Sci. Technol. 47 (2005) 126.

[13] T. Denner, K. H. Finken, G. Mank, N. Noda, Nucl. Fusion 39 (1999) 83.

[14] P. Wienhold, V. Philipps, A. Kirschner et al., J. Nucl. Mater. 313–316 (2003) 311.

[15] M. Mayer, P. Wienhold, D. Hildebrandt and W. Schneider, J. Nucl. Mater. 313–316 (2003) 377.

[16] A. Kreter, A. Kirschner, P. Wienhold et al., Phys. Scr. T128 (2007) 35.

[17] K. H. Finken, T. Denner, G. Mank, Nucl. Fusion 40 (2000) 339.

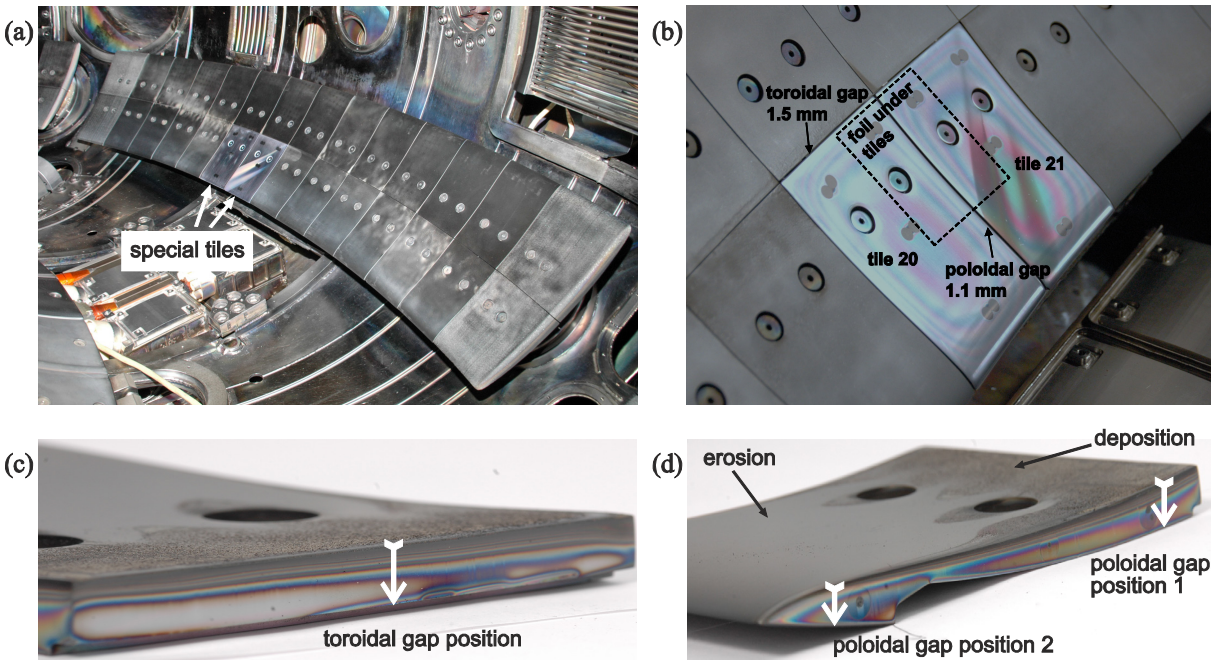

Fig. 1. (a) ALT-II blade with special tiles 20 and 21 prior to exposure, (b) special tiles 20 and 21 prior to exposure, the position of the foil covering the gap bottom between the tiles is schematically shown, (c) side wall of the toroidal gap of tile 20 after exposure, (d) side wall of the poloidal gap of tile 20 after exposure. Positions of analysis scans in Fig. 3 are indicated.

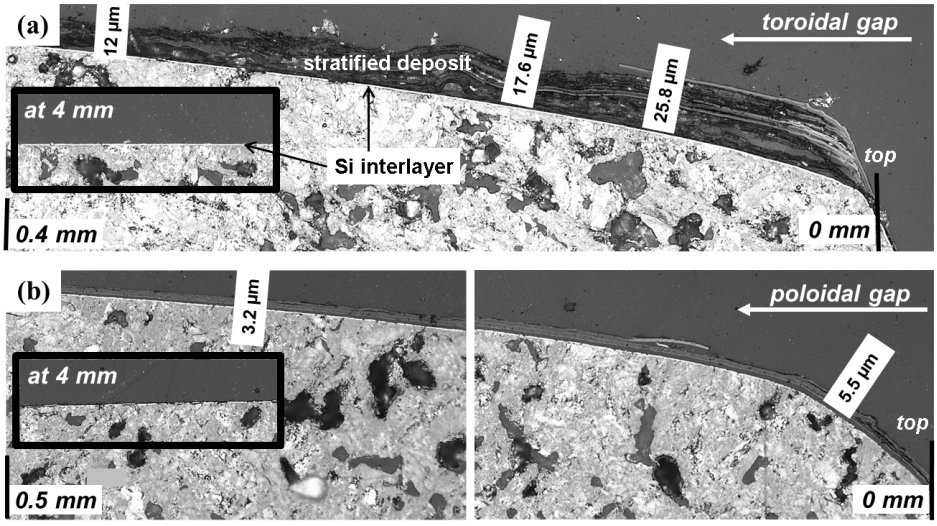

Fig. 2. Microscopic view of the cross-section (a) at the toroidal gap entrance of tile 21 and (b) at the poloidal gap entrance of tile 20. The stratified carbon deposit is well visible on the silicon interlayer (bright line), which lasts until the end of tile (insert at 4 mm). Distance from the gap entrance (in mm) and examples for thickness (in µm) are given.

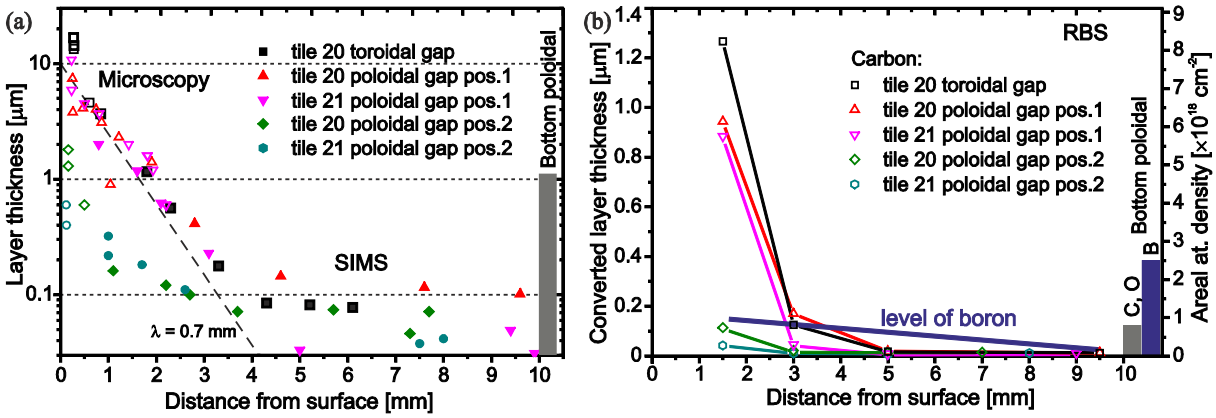

Fig. 3. (a) Layer thickness from the gap entrance to the bottom, measured by optical microscopy (open symbols) and SIMS (filled symbols). The broken line indicates the average decay length of the thickness of 0.7 mm. (b) RBS measurements of the areal atomic density (secondary Y axis), recalculated in the layer thickness (primary Y axis). The values at the gap bottom are shown as bars. The positions of measurements are indicated in Fig. 1.

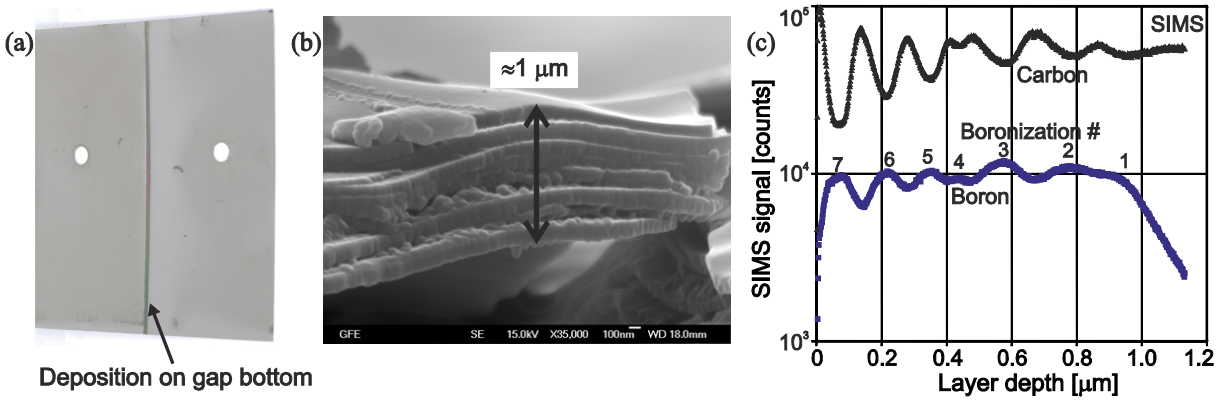

Fig. 4. (a) Foil under tiles 20 and 21 after exposure, (b) SEM of the layer peeled-off from the foil with a stratified structure, (c) SIMS depth profile of the deposition on the foil showing the anti-correlated signals of carbon from the tokamak operation and boron from the boronizations. All 7 boronizations during the campaign are visible.